electronics

MDPI

Article

Research on Predictive Speed Control Scheme for Surface-Mounted Permanent Magnet Servo Systems

Zhe Song [1,*], Weihong Zhou [1,2] and Yu Mo [3,4]

[1] Department of Electrical Engineering, Tsinghua University, Beijing 100084, China; 202221623249@smail.xtu.edu.cn
[2] College of Automation and Electronic Information, Xiangtan University, Xiangtan 411105, China
[3] School of Automation, Beijing Institute of Technology, Beijing 100081, China; moy@ht206.casic.com.cn
[4] Beijing Institute of Mechanical Equipment, Beijing 100854, China
* Correspondence: honghongshandong@hotmail.com

Abstract: In order to improve the dynamic response and disturbance rejection performance of electric machines, a deadbeat predictive speed control (DPSC) scheme for a permanent magnet synchronous motor (PMSM) is proposed. To begin with, a DPSC controller was proposed with the purpose of achieving precise control for the next control cycle, and the control parameters were determined based on the optimal parameter design method. For better application, performance comparisons were made with a conventional PI control, and the mismatch effects of inertia and torque were analyzed. In order to improve the disturbance rejection performance of the system, an extended sliding mode observer (ESMO) was constructed to compensate for disturbances. Experimental verification with a conventional PI control indicates that the proposed DPSC control can reduce the speed response time from 0.675 s to 0.650 s. When the electric machine operates stably and is applied to a torque disturbance of 0.4 Nm, the speed fluctuation and settling time can be reduced from 9 rpm and 1.7 s to 6 rpm and 0.5 s, respectively. This proposed method effectively enhances the speed control performance of PMSM and can be applied to high-performance electric machine applications.

Keywords: permanent magnet synchronous motor (PMSM); deadbeat predictive speed control (DPSC); extended sliding mode observer (ESMO); anti-load disturbance

check for updates

Citation: Song, Z.; Zhou, W.; Mo, Y. Research on Predictive Speed Control Scheme for Surface-Mounted Permanent Magnet Servo Systems. *Electronics* **2024**, *13*, 3421. https://doi.org/10.3390/electronics13173421

Academic Editor: Omid Beik

Received: 26 July 2024
Revised: 23 August 2024
Accepted: 23 August 2024
Published: 28 August 2024

Copyright: © 2024 by the authors. Licensee MDPI, Basel, Switzerland. This article is an open access article distributed under the terms and conditions of the Creative Commons Attribution (CC BY) license (https://creativecommons.org/licenses/by/4.0/).

1. Introduction

With its excellent performance, the permanent magnet synchronous motor (PMSM) has been widely applied in industrial robots, CNC machining centers, new energy vehicles, hydrogen fuel cells, wave power generation, wind power generation, and other fields [1–4]. It is an important component for realizing intelligent manufacturing and building new electrical power systems. In many application scenarios, when the dynamic response is high, the response time of the control system is shorter, which is beneficial for improving production efficiency. When the dynamic response is low, the control system cannot track fast speed commands, which can easily cause system oscillation, increase machining errors, and affect product quality. In addition, the PMSM operates in different states and environments, and the presence of motor parameters and external disturbances is inevitable, which affects the stability and control accuracy of the system. Therefore, in order to improve production efficiency and accuracy, it is necessary to improve the response speed and disturbance resistance performance of the PMSM control system.

The traditional PI control exhibits poor control performance when the system is subjected to internal parameter variations, such as resistance, inductance and flux, as well as external disturbances, such as load torque and inertia fluctuations [5]. In addition to PI control, there are many advanced control strategies used to improve the control performance of PMSM, such as sliding mode control [6,7], fuzzy control [8,9], predictive control [10,11], and intelligent control [12,13]. Among them, predictive control has become

a research hotspot in the field of motor control due to its excellent dynamic performance and significant potential.

According to the different control structures, predictive control can be divided into cascaded predictive control and non-cascaded direct predictive control [14]. Cascaded predictive control maintains the original dual-loop control structure, providing better stability. On the other hand, non-cascaded direct predictive control changes the original dual-loop control to a single-loop control, resulting in a faster dynamic response but increased sensitivity to parameter variations. Based on specific implementation principles, predictive control can be divided into model predictive control and deadbeat predictive control [15]. Model predictive control has relatively strong robustness but requires significant computation, leading to large current harmonics and speed ripples, as well as a complex weight factor design. On the other hand, deadbeat predictive control operates with a fixed switching frequency, simple algorithm, lower computational load, and smaller ripples, and exhibits good tracking performance and a dynamic response. Based on the different control objectives, predictive control can also be classified into current predictive control and speed predictive control [16], with the former having been developed earlier and having relatively mature research.

In this control strategy, employing advanced predictive control in the current loop can enhance the current dynamic performance of PMSM. However, due to the limitations of classical control methods in the outer speed loop, the improvement in speed control performance is not significant, which further impacts the position servo and industrial applications [17]. The emergence of speed predictive control has provided an effective method for improving the control performance of the speed loop and has become a new research hotspot. However, similar to other predictive control methods, the performance of speed predictive control also relies on the parameters of the PMSM system. In order to reduce the impact of internal parameters and external disturbances on dynamic response and steady-state errors, various methods are typically employed for improvement, such as parameter identification [18], precise modeling [19], a Luenberger observer [20], a sliding mode observer [21], and a Kalman filter [22]. Parameter identification can accurately identify system parameters but it has a relatively poor disturbance rejection capability. Accurate modeling can enhance the robustness of the system but it increases the complexity of the algorithm and makes it difficult to account for unmodeled dynamics. The Luenberger observer has a fast response and small error but it is susceptible to the effects of parameter mismatch. The Kalman filter has a high disturbance rejection capability and accuracy but it has a complex algorithm and requires a large computational load. The sliding mode observer has a low requirement for model accuracy, strong robustness to parameter perturbation and external perturbation, and is easy to implement, making it an increasingly popular research topic [23–25].

Reference [26] proposed a deadbeat predictive current control method. In order to solve the problem of parameter mismatch in the PMSM model, the least squares method is used to identify the electromagnetic parameters. To improve the response of current control and reduce the influence of parameter fluctuations, reference [27] proposed a deadbeat predictive current control method with integral disturbance feed-forward. In order to reduce the sensitivity of parameter errors in deadbeat predictive current control, reference [28] used extended Kalman filter compensation to reduce the impact of disturbances and parameter mismatches. These articles have improved control performance from different aspects. However, the combination of deadbeat predictive current control and a PI speed controller will affect the overall control performance of the system.

On the other hand, model predictive direct speed control using the non-cascaded control structure for direct speed prediction control can avoid the influence of the outer speed loop and directly achieve speed prediction control. A model predictive direct speed control method for PMSM was proposed in [29], and an SMO observer was formulated to compensate for the reference voltage error caused by parameter disturbances. Reference [30] proposed a speed-predictive control method with online adjustment of weight

factors. By constructing a new cost function, the speed dynamics have been improved. A model predictive direct speed control was proposed for PMSM in [15], equipped with a novel dual second-order SMO observer, improving the robustness and high bandwidth of the control system. However, these control methods adopt a non-cascaded control structure, which can easily generate a large current and speed ripples, reducing the stability of the control system. Meanwhile, these methods control both current and speed simultaneously, resulting in an increased computational burden on the controller.

In response to the research status and issues above, this paper proposes a deadbeat predictive speed control (DPSC) method with an extended sliding mode observer (ESMO) for a surface-mounted permanent magnet synchronous motor (SPMSM). In order to improve the dynamic performance of the speed loop while maintaining good stability, a cascade structure-based DPSC control method is proposed. The design method and principles for parameter selection of this controller are provided. The control performance of this method was compared with a PI controller as a reference. The impact of external disturbances (inertia and torque errors) on the control performance was analyzed, and an ESMO was designed to enhance the disturbance rejection capabilities. Finally, the effectiveness of the proposed method was verified through experiments. The designed DPSC controller and ESMO observer improved the parameter robustness of predictive control.

The remainder of this article is organized as follows. Section 2 introduces the deadbeat predictive speed control of PMSM. In Section 3, a comparative analysis is conducted with PI control, and the impact of parameter mismatch is also studied. Subsequently, the ESMO torque observer is designed in Section 4. The experimental testing and validation are presented in Section 5. Section 6 concludes this paper.

2. Deadbeat Predictive Speed Control

2.1. DPSC Controller Design

According to the working principle of SPMSM, its dynamic equation can be expressed as follows [31–33]:

$$\begin{cases} \frac{d\boldsymbol{x}}{dt} = \boldsymbol{A}\boldsymbol{x} + \boldsymbol{B}u \\ y = \boldsymbol{C}\boldsymbol{x} \end{cases} \tag{1}$$

where $\boldsymbol{x} = \begin{bmatrix} \omega_{\mathrm{m}} \\ T_{\mathrm{L}} \end{bmatrix}$, $\boldsymbol{A} = \begin{bmatrix} \frac{-B_{\mathrm{m}}}{J_{\mathrm{m}}} & \frac{-1}{J_{\mathrm{m}}} \\ 0 & 0 \end{bmatrix}$, $\boldsymbol{B} = \begin{bmatrix} \frac{1}{J_{\mathrm{m}}} \\ 0 \end{bmatrix}$, $\boldsymbol{C}$ = [1 0], u = T_{e}, $y = \omega_{\mathrm{m}}$.

In the formula, ω_{m} represents the mechanical angular velocity of the rotor, T_{L} represents the load torque of the motor, B_{m} represents the viscous friction coefficient, J_{m} represents the rotational inertia of the motor, and T_{e} represents the electromagnetic torque of the motor.

According to the Newton motion Equation (1) of the PMSM, using the forward Euler method for discretization, it can be obtained that:

$$T[k_t i_q^* - T_L(k) - B_m\omega_m(k)] = J_m[\omega_m(k+1) - \omega_m(k)] \tag{2}$$

where T is the control period and k_t is the motor torque constant.

In order to improve the control performance, predictive control is used to follow the speed value of the next control period (k + 1) T within the present control period kT. To enable the motor speed to track the speed command of the present period, if $\omega_m(k+1) = \omega_m^*(k)$ is taken while neglecting the viscous friction coefficient B_{m}, the control law for DPSC can be obtained as follows:

$$i_q^* = \frac{J_m}{Tk_t}[\omega_m^*(k) - \omega_m(k)] + \frac{T_L(k)}{k_t} \tag{3}$$

where $\omega_m^*(k)$ is the velocity setpoint at time k.

2.2. Determination of Control Parameters

In practical applications, the system inertia cannot be accurately obtained. Therefore, the control parameter $\frac{J_m}{Tk_t}$ for DPSC can be denoted as k_s, as shown in Figure 1. In the diagram, $G_{ic}(s)$ represents the transfer function of the current loop, while i_q^* and i_q respectively denote the current reference value and the actual value.

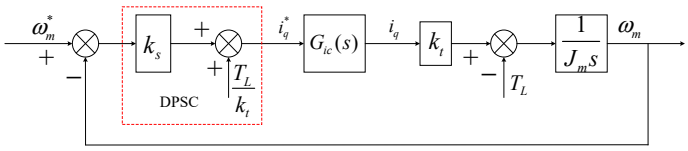


Figure 1. Deadbeat predictive speed control block diagram.

Since the adjustment process of the current loop is faster than that of the speed loop, it can be equivalently represented as a first-order inertia link. By taking $G_{ic}(s) = \frac{1}{2Ts+1}$, the input–output transfer function $G_\omega(s)$ and torque disturbance–output transfer function $G_{TL}(s)$ of the DPSC control system can be obtained as follows:

$$G_\omega(s) = \frac{\omega_m}{\omega_m^*} = \frac{k_s k_t}{2TJ_m s^2 + J_m s + k_s k_t} \tag{4}$$

$$G_{TL}(s) = \frac{\omega_m}{T_L} = -\frac{2Ts}{2TJ_m s^2 + J_m s + k_s k_t} \tag{5}$$

From the system control structure and transfer function (4) and (5), it is well known that a larger value of k_s can make the system more responsive and quicker, but an excessively large k_s value will lead to system oscillation and instability. Pursuant to the principles of automatic control, the stability of a system is directly correlated with the positioning of the poles within the closed-loop transfer function. Based on the open-loop transfer function, in order to achieve optimal stability and dynamic, the parameter and damping ratio must be met.

$$\begin{cases} \frac{k_s k_t}{J_m} 2T = 0.5 \\ \xi = 0.707 \end{cases} \tag{6}$$

where ξ is the damping ratio.

In the system, the control frequency is 10 kHz, the motor torque constant k_t is 1, and the rotational inertia J_m is 2.34 × 10^{-3} kg·m^2, so the DPSC control parameter k_s can be calculated as 5.85 from Equation (6).

The plot root locus of the system as shown in Figure 2. From the graph, it can be seen that the intersection point of the root locus and $\xi = 0.707$ is to the optimal closed-loop pole. The intersection pole is $s_{1,2} = -2500 \pm 2500$ i, with a gain of $k_s k_t$ as 5.85. Therefore, based on the value of $k_t = 1$, the corresponding control parameter k_s is further confirmed to be 5.85.

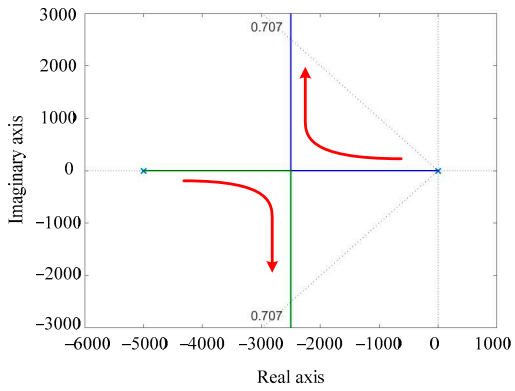


Figure 2. Control system root locus: blue and green represent root trajectories, and red represents the trend of root trajectory changes.

3. Control Performance Analysis

3.1. Comparison of Control Performance

In order to rigorously demonstrate the effectiveness of the proposed DPSC control methodology, a comparative analysis has been undertaken with the conventional PI control mechanism. Figure 3 presents the block diagram of the PI speed control system, wherein k_p and k_i represent the proportional and integral coefficients of the PI speed controller, respectively.

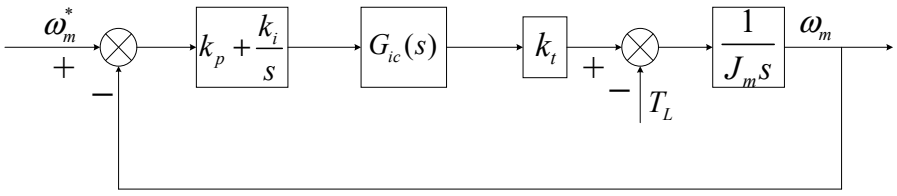


Figure 3. Block diagram of the PI speed control system.

Similarly, taking the closed-loop transfer function of the current loop as $G_{ic}(s) = \frac{1}{2Ts+1}$, the input–output transfer function $G_\omega(s)$ and the torque disturbance–output transfer function $G_{TL}(s)$ for the system under traditional PI speed control can be obtained as follows:

$$G_\omega(s) = \frac{\omega_m}{\omega_m^*} = \frac{k_p k_t s + k_i k_t}{2TJ_m s^3 + J_m s^2 + k_p k_t s + k_i k_t} \tag{7}$$

$$G_{TL}(s) = \frac{\omega_m}{T_L} = -\frac{2Ts^2 + s}{2TJ_m s^3 + J_m s^2 + k_p k_t s + k_i k_t} \tag{8}$$

When using PI speed control, its transfer function can be denoted as follows:

$$G_s(s) = k_p + \frac{k_i}{s} \tag{9}$$

where $k_i = \frac{k_p}{\tau}$ and τ represent the integral time constants.

Following the typical Type-II system, apply the third-order optimal design method to design the PI control parameters:

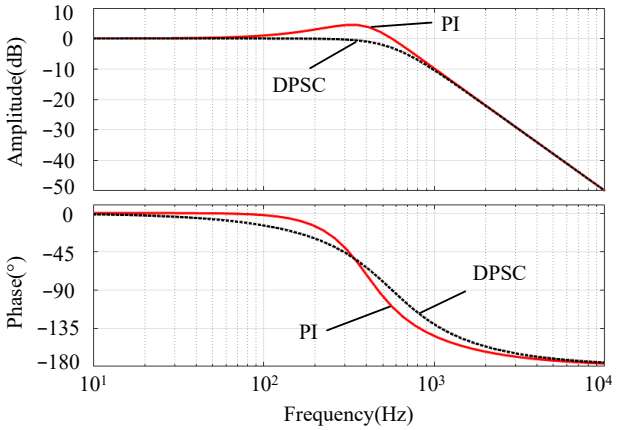
$$\begin{cases} \tau = h \times 2T \\ \frac{k_p k_t}{\tau J_m} = \frac{1}{2h \times (2T)^2} \end{cases} \tag{10}$$

where h is the mid-frequency bandwidth. As the system has the shortest settling time when h = 4, it is chosen accordingly and substituted into Equation (10) above. Similarly, with the system control frequency set at 10 kHz, the motor torque constant k_t as 1, and the rotational inertia J_m as 2.34 × 10^{-3} kg·m^2, the numerical values of k_p and k_i can be calculated as 5.85 and 7312.5, respectively.

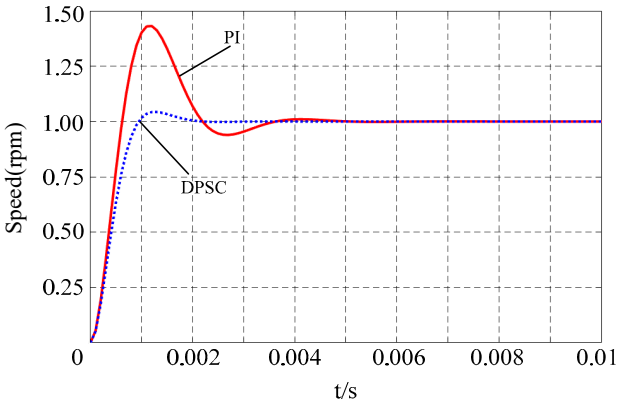
To compare and analyze the performance of different speed control methods, under the optimal control parameters, i.e., taking k_s = 5.85, k_p = 5.85, and k_i = 7312.5, and substituting the motor parameters from Table 1 into Equations (4) and (7), the Bode plot and speed response curve of the system under the proposed DPSC and conventional PI control are obtained for the reference speed as a unit step input, as shown in Figure 4.

Table 1. PMSM motor parameters.

Parameters	Value	Parameters	Value
Rated power (kW)	3	Stator inductance (mH)	23.1
Rated torque (Nm)	5	Stator resistance (Ω)	1.386
Rated speed (rpm)	1500	Rotational inertia (kg·m^2)	2.34×10^{-3}
Rated current (A)	5	Friction coefficient (N·s/m)	3.01×10^{-3}
Number of pole pairs	2		



(**a**) Bode plot of the transfer function.

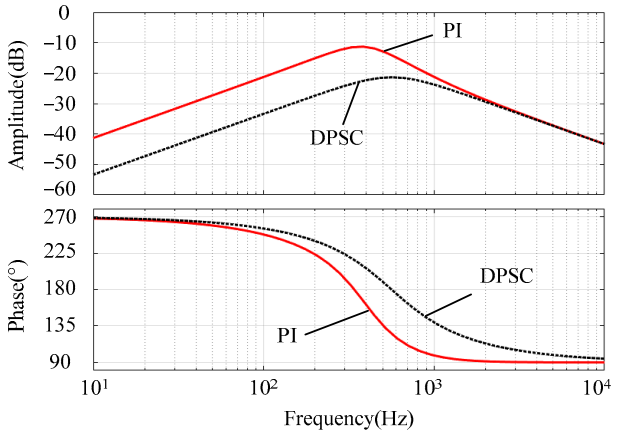


(**b**) Step response of speed.

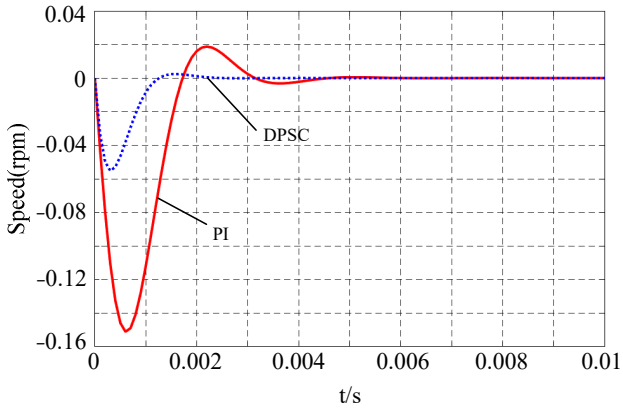
Figure 4. Speed transfer function control curve.

From the Bode graph in Figure 4a, it can be seen that the control frequency for the DPSC with a phase lag of $-90°$ is about 600 Hz, while the frequency for the PI control with a phase lag of $-90°$ is about 500 Hz. It is obvious that the bandwidth of the DPSC is significantly higher than that of the PI control, with a faster dynamic response. As shown in Figure 4b, when a step reference speed is input, the speed overshoot of the traditional PI is relatively large. When using DPSC speed predictive control, the speed overshoot is basically zero, and the system exhibits a faster dynamic response and shorter settling time.

Similarly, by substituting the motor parameters from Table 1 into Equations (5) and (8), the Bode plot and speed response curve of the system under the disturbance input of a unit step load torque for the two different control methods are obtained, as shown in Figure 5. From the graph, it can be seen that compared to traditional PI speed control, DPSC speed predictive control shows improved disturbance rejection capability against load disturbances, allowing the system to recover to a stable state more rapidly.



(**a**) Bode plot of the transfer function.



(**b**) Step response of speed.

Figure 5. Torque transfer function control curve.

3.2. Parameter Mismatch Impact

Due to the mismatch errors in the actual parameters of inertia and load torque in speed control, in order to analyze the impact of inertia error and load torque error on the speed control output i_q^*, control law models containing inertia error and load torque error are established separately.

When there is a mismatch error in the inertia, denoted as J_m', Equation (3) of control law for DPSC becomes

$$i_q^{*\prime} = \frac{J_m'}{Tk_t}[\omega_m^*(k) - \omega_m(k)] + \frac{T_L(k)}{k_t} \tag{11}$$

Subtracting Equation (11) from Equation (3), the current dynamic error can be obtained as follows:

$$\Delta i_q^* = \frac{\Delta J_m}{Tk_t}[\omega_m^*(k) - \omega_m(k)] \tag{12}$$

where $\Delta J_m = J_m - J_m'$ represents the difference between the actual inertia J_m and the modeled inertia J_m'.

Through Equation (12), it can be observed that the inertia error will have a certain impact on the output i_q^* of DPSC control. Plot the error in i_q^* generated by inertia errors of ±30%, as shown in Figure 6. In the analysis of Figure 6, it is discernible that under a specified rate of change in angular velocity, the magnitude of the current error escalates in tandem with an augmentation in the inertia error. Conversely, maintaining a constant level of inertia error, the current error exhibits a corresponding growth as the angular velocity change rate intensifies. In this system, the maximum value of the i_q^* error caused by the inertia error is 0.0702 A.

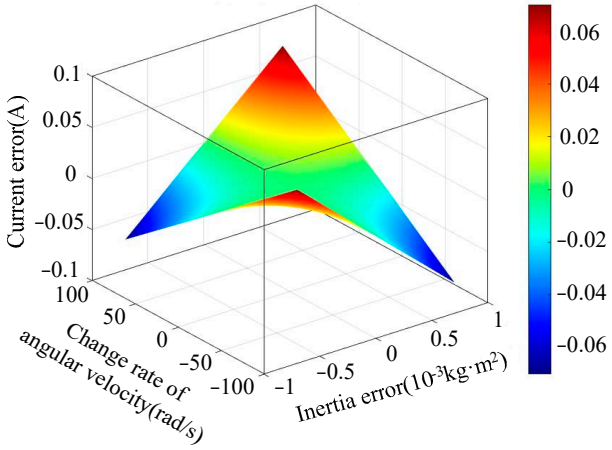


Figure 6. The impact of inertia error on predictive control.

Similarly, when there is a deviation in the load torque, denoted as T_L', the control law for DPSC becomes

$$i_q^{*\prime} = \frac{J_m}{Tk_t}[\omega_m^*(k) - \omega_m(k)] + \frac{T_L'(k)}{k_t} \tag{13}$$

Subtracting Equation (13) from Equation (3), the current dynamic error can be obtained as follows:

$$\Delta i_q^* = \frac{\Delta T_L}{k_t} \tag{14}$$

where $\Delta T_L = T_L - T_L'$ represents the difference between the actual torque T_L and the modeled torque T_L'.

Through Equation (14), plot the error in i_q^* generated by the load torque errors of ±30%, as shown in Figure 7. Analyzing Figure 7, it can be observed that when the torque error is constant, the current error increases as the torque coefficient decreases; and when the torque coefficient is constant, the current error increases with the increase of the torque error. Specifically, when the torque coefficient k_t is 1, the maximum value of the i_q^* error caused by the load torque error is 1.5 A.

From the analysis above, it can be seen that both the inertia and torque parameter errors affect the predictive control output i_q^*, but the i_q^* is more sensitive to torque errors. To improve control accuracy, in system design, the primary consideration should be to reduce the impact of torque error on speed predictive control.

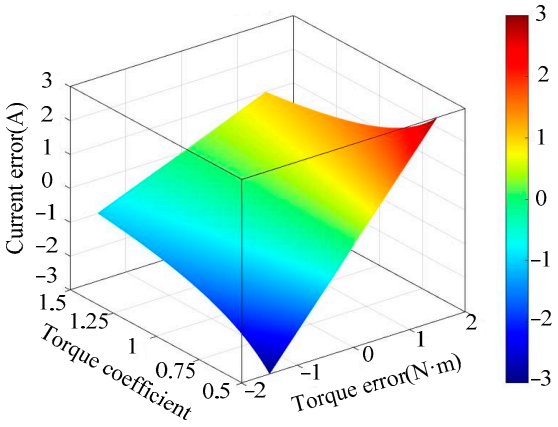


Figure 7. The impact of torque error on predictive control.

4. ESMO Torque Observer

4.1. The Observer Design

To mitigate the impact of torque error on DPSC control and enhance the system's resilience against load disturbances, an extended sliding mode observer (ESMO) is formulated to observe and compensate for load torque. The sliding surface is defined as the error between the estimated speed and the actual speed, denoted as $S = \hat{\omega}_e - \omega_e$, and the constant convergence rate is adopted. Furthermore, to enhance the system's dynamic performance, a continuous function *sigmoid*(*s*) is used instead of the sign function *sign*(s) in conventional reaching law, and the expression is as follows:

$$U = K \cdot sigmoid(s) \tag{15}$$

where K is the control parameter of the *sigmoid*(s).

According to the principle of Equation (1) of PMSM, the ESMO can be formulated as follows:

$$\begin{cases} \frac{d\hat{\omega}_e}{dt} = \frac{n_p(T_e - \hat{T}_L)}{J_m} + U \\ \frac{d\hat{T}_L}{dt} = gU \end{cases} \tag{16}$$

where g represents the sliding mode parameter and $\hat{T}_L$ represents the observed load. The observation principle of ESMO is shown in Figure 8.

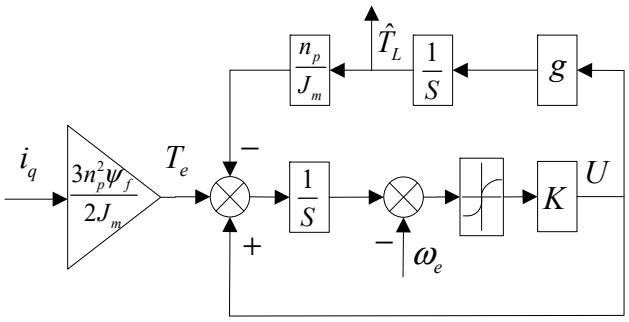


Figure 8. ESMO observation principle block diagram.

To ensure the sliding mode control reaches the sliding surface rapidly and stably, it is necessary to design the observer parameters reasonably. The error equations for speed and torque are defined as follows:

$$\begin{cases} s_1 = \hat{\omega}_e - \omega_e \\ s_2 = \hat{T}_L - T_L \end{cases} \tag{17}$$

Since the load torque T_L has a relatively high sampling frequency, it can be considered as a constant within one sampling period. From Equation (16), the error differential equation can be derived as follows:

$$\begin{cases} \frac{ds_1}{dt} = -\frac{n_p s_2}{J_m} + U \\ \frac{ds_2}{dt} = gU \end{cases} \tag{18}$$

To ensure the stability of the system, it is necessary to satisfy the Lyapunov stability equation:

$$\begin{aligned} S\dot{S} &= S\frac{dS}{dt} = s_1\frac{ds_1}{dt} \\ &= s_1\left[-\frac{n_p s_2}{J_m} + K \cdot sigmoid(s)\right] \le 0 \end{aligned} \tag{19}$$

Thus, the range of values for K can be obtained as follows:

$$K \le -\left|\frac{n_p s_2}{J_m}\right| \tag{20}$$

Designing a reasonable value for K can help the system reach the sliding surface quickly, while ensuring that the sliding surface S and its derivative satisfy the following:

$$\begin{cases} S = \frac{dS}{dt} = 0 \\ s_1 = \frac{ds_1}{dt} = 0 \end{cases} \tag{21}$$

Substituting the equation above into Equation (18) yields the following:

$$\frac{ds_2}{dt} - g\frac{n_p s_2}{J_m} = 0 \tag{22}$$

To ensure the convergence of the torque observation error to zero, the Lyapunov stability equation should be satisfied.

$$s_2 \frac{ds_2}{dt} \leq 0 \tag{23}$$

By substituting (23) into Equation (22), it can be derived that the sliding mode parameter g should be less than or equal to zero. It is evident that when g equals zero, the constructed ESMO Equation (16) becomes meaningless, hence parameter g should satisfy the condition $g < 0$.

4.2. Principle of System Control

In speed predictive control, torque observation is introduced and updated into the DPSC controller to enhance the control performance of the system. By substituting the identified torque value $\hat{T}_L$ obtained from the observer into Equation (3), the control law for speed predictive control with ESMO can be derived as follows:

$$i_q^* = \frac{J_m}{Tk_t}[\omega_m^*(k) - \omega_m(k)] + \frac{\hat{T}_L(k)}{k_t} \tag{24}$$

After the torque observation and update described above, the schematic diagram of the DPSC control method with ESMO proposed in this paper is shown in Figure 9.

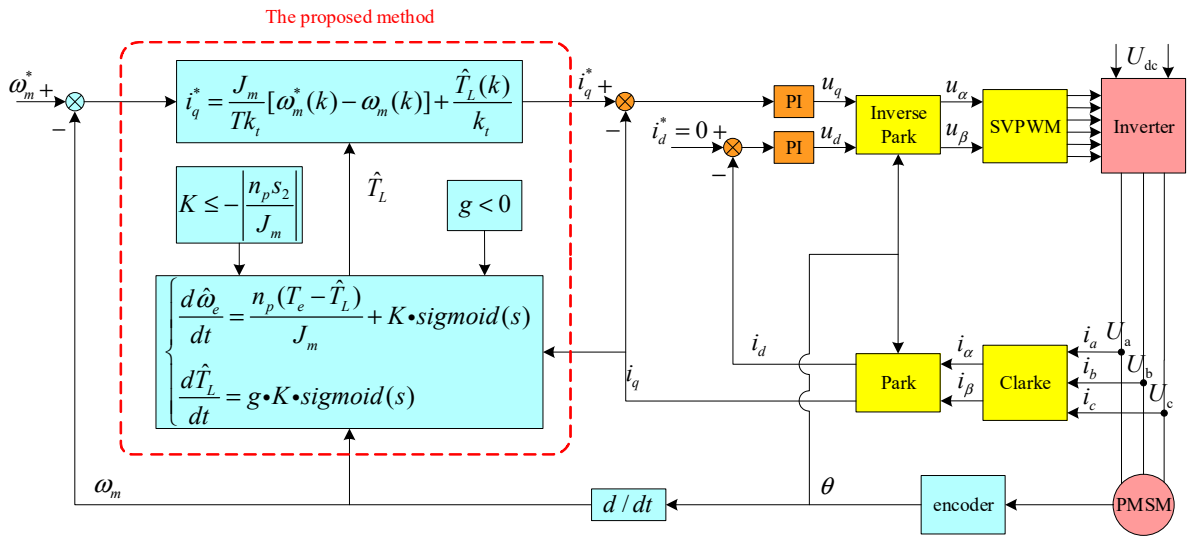


Figure 9. Adaptive deadbeat predictive speed control.

5. Experimental Research

The experimental platform includes a MT1050 controller from Shanghai Yuan Kuan Energy Technology Co., Ltd., Shanghai, China, with TMS320F28335 as the main control chip, a PMSM motor from Hebei Electric Machinery Co., Ltd., Cangzhou, China, and a load

motor, torque sensor, and upper computer, as shown in Figure 10. The driver is powered by 380 V DC, and the switching frequency of the inverter is 10 kHz. The motor used is fully consistent with the theoretical analysis, and its parameters are listed in Table 1. In the experiment, the same PI current controller is used, with parameters k_s = 5.85, k_p = 5.85, and k_i = 7312.5 for the speed controller.

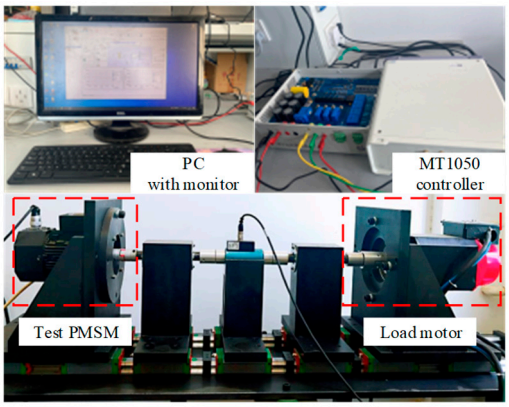


Figure 10. PMSM drive control system.

5.1. Observer Performance Analysis

Figure 11 shows the waveform output of the ESMO observer. The motor's specified speed is 1000 rpm, which is equivalent to an electrical angular velocity of 209.44 rad/s. Due to mechanical installation errors, the experimental system has inherent friction and damping of 1.1 Nm, with an additional load torque of 4 Nm applied during the experiment. From the top to bottom of Figure 11 are the actual angular velocity, estimated angular velocity, and estimated load torque of the ESMO, respectively. It can be seen that the designed ESMO observer is capable of accurately observing the load torque and electrical angular velocity. The estimated angular velocity can follow the actual angular velocity with high accuracy and a consistent trend of change. The response of the estimated load torque is fast, and the error is small. The convergence time for torque observation is 690 ms with an error of 3.89%, which can provide disturbance compensation for speed control.

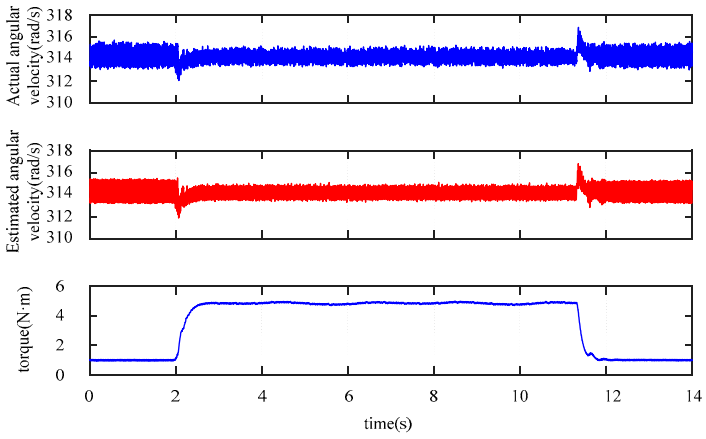
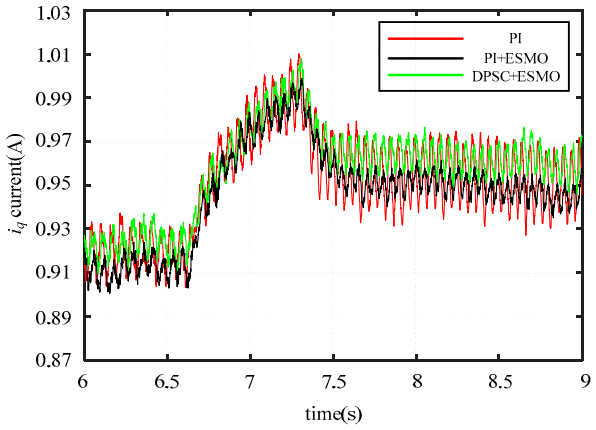


Figure 11. ESMO torque observation waveform.

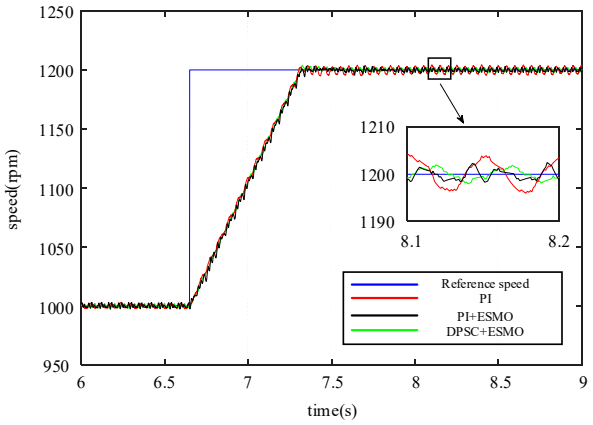
5.2. Dynamic Response Analysis

To validate the effectiveness of the proposed method, three control methods are compared: conventional PI control, PI control with disturbance compensation (PI + ESMO), and disturbance compensated deadbeat predictive speed control (DPSC + ESMO). The PMSM is started and operated with a load torque of 1.1 Nm at a reference speed of 1000 rpm. Figure 12 shows the experimental waveforms for different control methods. Based on the

analysis of the response depicted in Figure 12a, it is evident that the i_q current of the PI control exhibits significant fluctuations, followed by a lesser degree of fluctuation of the PI + ESMO, and the DPSC + ESMO control exhibits the minimal current fluctuation. Meanwhile, as shown in Figure 12b, the response time of conventional PI is 0.675 s with no overshoot and a speed fluctuation of 4 rpm; PI + ESMO has a response time of 0.675 s, also with no overshoot and a speed fluctuation of 3 rpm; DPSC + ESMO has a response time of 0.65 s, likewise with no overshoot and a speed fluctuation of 2 rpm. Table 2 provides the comparative data. It is evident that the proposed DPSC + ESMO method can improve the system's dynamic response, effectively reduce the settling time and speed fluctuation, and enhance speed tracking performance.



(**a**) Current response.



(**b**) Speed response.

Figure 12. Dynamic response of different control methods.

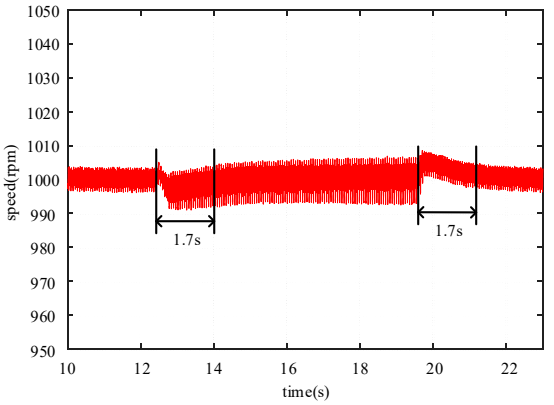
Table 2. Experimental results of speed response.

Control Method	Settling Time	Fluctuate Error
PI	0.675 s	4 rpm
PI + ESMO	0.675 s	3 rpm
DPSC + ESMO	0.65 s	2 rpm

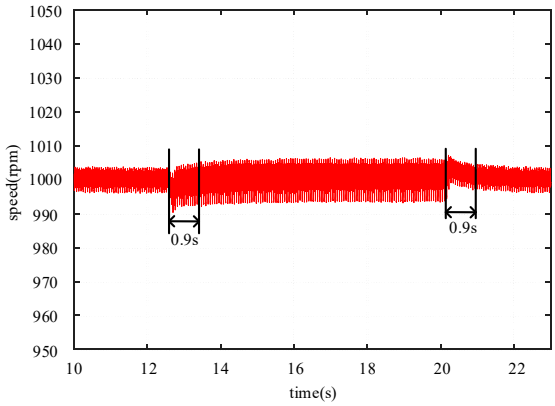
5.3. Disturbance Rejection Performance Analysis

The PMSM is started and operated at a reference speed of 1000 rpm with a load torque of 1.1 Nm. After reaching stability, a sudden additional load torque of 0.4 Nm is applied to the system until it stabilizes again. Subsequently, the load is removed to restore the torque to its original 1.1 Nm level. The experimental waveform is shown in Figure 13. From the figure, it can be observed that the maximum speed fluctuation for conventional PI is 9 rpm with a recovery time of 1.7 s; for PI + ESMO, the maximum speed fluctuation is

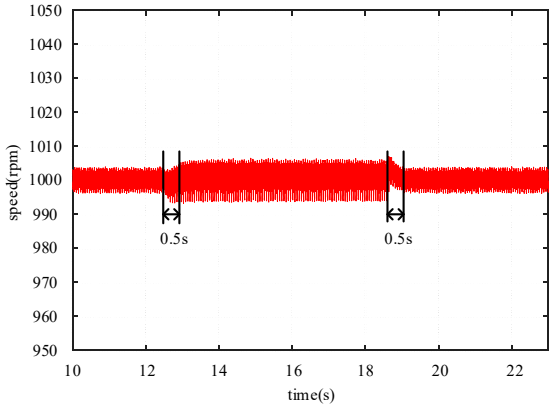
9 rpm with a recovery time of 0.9 s; and for DPSC + ESMO, the maximum speed fluctuation is 6 rpm with a recovery time of 0.5 s. Table 3 provides the comparative data. It can be seen that when subjected to disturbance, the proposed DPSC + ESMO method is able to reduce speed fluctuation and recovery time, thus improving the system's disturbance rejection performance.



(**a**) PI control method.



(**b**) PI + ESMO control method.



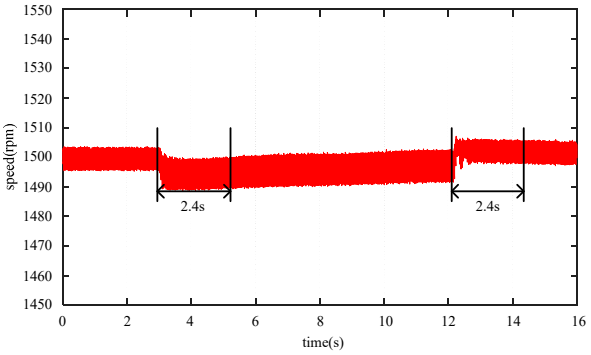
(**c**) DPSC + ESMO control method.

Figure 13. Speed waveform of 0.4 Nm load change.

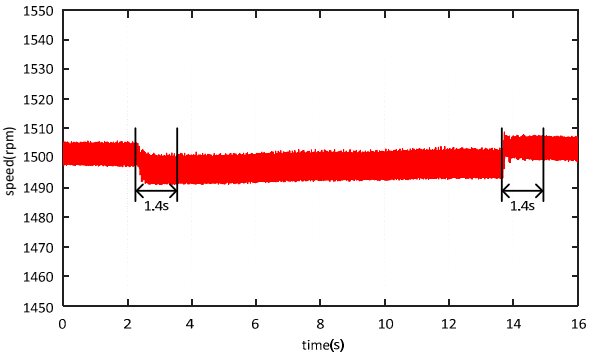
Table 3. Experimental results of 0.4 Nm load disturbance rejection.

Control Method	Overshoot	Settling Time
PI	9 rpm	1.7 s
PI + ESMO	9 rpm	0.9 s
DPSC + ESMO	6 rpm	0.5 s

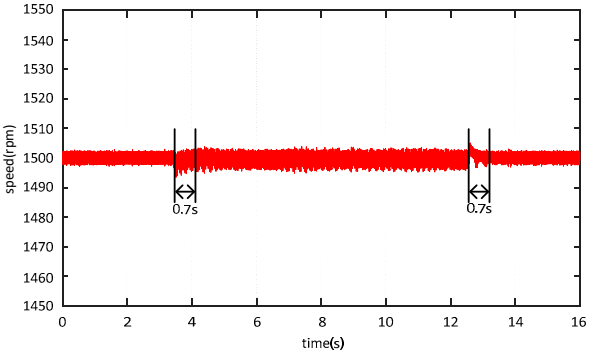
To further validate the performance of the proposed method, experimental research was conducted near the rated load. The PMSM is stable when operated at a reference speed of 1000 rpm with a load torque of 1.1 Nm, and a sudden additional load torque of 4 Nm is applied to the system. Subsequently, the load is removed to restore the PMSM to the original 1.1 Nm level. The experimental waveform is shown in Figure 14. It can be observed that the maximum speed fluctuation for conventional PI is 12 rpm with a recovery time of 2.4 s; for PI + ESMO, the maximum speed fluctuation is 9 rpm with a recovery time of 1.4 s; and for DPSC + ESMO, the maximum speed fluctuation is 7 rpm with a recovery time of 0.7 s. Table 4 provides the comparative data.



(**a**) PI control method.



(**b**) PI + ESMO control method.



(**c**) DPSC + ESMO control method.

Figure 14. Speed waveform of 4 Nm load change.

Table 4. Experimental results of 4Nm load disturbance rejection.

Control Method	Overshoot	Settling Time
PI	12 rpm	2.4 s
PI + ESMO	9 rpm	1.4 s
DPSC + ESMO	7 rpm	0.7 s

From the experimental results above, it can be seen that the proposed DPSC method with ESMO has a better dynamic response and disturbance resistance performance than traditional PI. This is because DPSC speed control does not have an integral term, which reduces the damping effect, expands the system bandwidth, and improves the dynamic response. Meanwhile, utilizing ESMO to observe disturbances and updating them into the controller for torque compensation improves the system's disturbance resistance performance.

6. Conclusions

We have proposed a PMSM deadbeat predictive speed control (DPSC) method with an extended sliding mode observer (ESMO). The design method and parameter selection principles of the controller are provided, and the effects of inertia error and torque error on the control performance are analyzed. An ESMO observer is designed to observe and compensate for the load torque. The following conclusions are drawn through theoretical analysis and experimental research:

1. The inertia error and torque error have corresponding effects on the deadbeat predictive speed control. Specifically, the current error of the predictive control output increases with the increase of the inertia error and torque error, but is more significantly influenced by torque error, being more sensitive to it.
2. The designed ESMO observer can rapidly and accurately observe the load torque, with a fast dynamic response to track load changes and small steady-state error. The observation accuracy is 94.37%, which can provide disturbance compensation for speed control.
3. The DPSC control method with an ESMO observer can effectively improve the system's dynamic response and disturbance rejection performance. Compared to conventional PI control, the speed step response time is reduced from 0.675 s to 0.650 s, and when subjected to a load disturbance of 0.4 Nm, the speed fluctuation and settling time decrease from 9 rpm and 1.7 s to 6 rpm and 0.5 s, respectively.
4. The method proposed in this article has significant theoretical significance for improving the control performance of an SPMSM speed system and can be applied to control scenarios with fast speed response requirements, such as industrial robots, CNC machine tools, and electric vehicles.

Author Contributions: Conceptualization, Z.S.; methodology, Z.S.; software, W.Z.; validation, W.Z.; formal analysis, Y.M.; investigation, Y.M.; resources, Y.M.; data curation, Z.S.; writing—original draft preparation, Z.S.; writing—review and editing, W.Z.; visualization, Y.M.; project administration, Y.M.; funding acquisition, Z.S. All authors have read and agreed to the published version of the manuscript.

Funding: This work was supported in part by the National Key Research and Development Project of China under Grant 2020YFE0205400, and in part by the National Natural Science Foundation of China under Grant 52337002 and Grant 52305541.

Data Availability Statement: The data presented in this study are available on request from the corresponding authors.

Acknowledgments: Thanks to all the Project team members.

Conflicts of Interest: The authors declare no conflict of interest.

References

1. Qiu, Z.; Chen, Y.; Kang, Y.; Liu, X.; Gu, F. Investigation into periodic signal-based dithering modulations for suppression sideband vibro-acoustics in PMSM used by electric vehicles. *IEEE Trans. Energy Convers.* **2020**, *36*, 1787–1796. [CrossRef]
2. Sun, Y.; Yang, M.; Wang, B.; Chen, Y.; Xu, D. Precise position control based on resonant controller and second-order sliding mode observer for PMSM-driven feed servo system. *IEEE Trans. Transp. Electrif.* **2022**, *9*, 196–209. [CrossRef]
3. Zhao, T.; Wu, S.; Cui, S. Multiphase PMSM with asymmetric windings for more electric aircraft. *IEEE Trans. Transp. Electrif.* **2020**, *6*, 1592–1602. [CrossRef]

4. Fang, S.; Wang, Y.; Wang, W.; Chen, Y.; Chen, Y. Design of permanent magnet synchronous motor servo system based on improved particle swarm optimization. *IEEE Trans. Power Electron.* **2021**, *37*, 5833–5846. [CrossRef]
5. Wu, J.; Zhang, J.; Nie, B.; Liu, Y.; He, X. Adaptive control of PMSM servo system for steering-by-wire system with disturbances observation. *IEEE Trans. Transp. Electrif.* **2021**, *8*, 2015–2028. [CrossRef]
6. Wang, Y.; Feng, Y.; Zhang, X.; Liang, J. A new reaching law for antidisturbance sliding-mode control of PMSM speed regulation system. *IEEE Trans. Power Electron.* **2019**, *35*, 4117–4126. [CrossRef]
7. Xu, W.; Junejo, A.K.; Liu, Y.; Hussien, M.G.; Zhu, J. An efficient antidisturbance sliding-mode speed control method for PMSM drive systems. *IEEE Trans. Power Electron.* **2020**, *36*, 6879–6891. [CrossRef]
8. Vadivel, R.; Joo, Y.H. Reliable fuzzy H_∞ control for permanent magnet synchronous motor against stochastic actuator faults. *IEEE Trans. Syst. Man Cybern. Syst.* **2019**, *51*, 2232–2245. [CrossRef]
9. Mani, P.; Rajan, R.; Shanmugam, L.; Joo, Y.H. Adaptive fractional fuzzy integral sliding mode control for PMSM model. *IEEE Trans. Fuzzy Syst.* **2018**, *27*, 1674–1686. [CrossRef]
10. Gao, S.; Wei, Y.; Zhang, D.; Qi, H.; Wei, Y.; Yang, Z. Model-free hybrid parallel predictive speed control based on ultralocal model of PMSM for electric vehicles. *IEEE Trans. Ind. Electron.* **2022**, *69*, 9739–9748. [CrossRef]
11. Li, Z.; Wang, F.; Ke, D.; Li, J.; Zhang, W. Robust continuous model predictive speed and current control for PMSM with adaptive integral sliding-mode approach. *IEEE Trans. Power Electron.* **2021**, *36*, 14398–14408. [CrossRef]
12. Nguyen, T.T.; Tran, H.N.; Nguyen, T.H.; Jeon, J.W. Recurrent neural network-based robust adaptive model predictive speed control for PMSM with parameter mismatch. *IEEE Trans. Ind. Electron.* **2022**, *70*, 6219–6228. [CrossRef]
13. Hang, J.; Shu, X.; Ding, S.; Huang, Y. Robust open-circuit fault diagnosis for PMSM drives using wavelet convolutional neural network with small samples of normalized current vector trajectory graph. *IEEE Trans. Ind. Electron.* **2023**, *70*, 7653–7663. [CrossRef]
14. He, L.; Wang, F.; Wang, J.; Rodríguez, J. Zynq implemented Luenberger disturbance observer based predictive control scheme for PMSM drives. *IEEE Trans. Power Electron.* **2019**, *35*, 1770–1778. [CrossRef]
15. Li, S.; Xu, Y.; Zhang, W.; Zou, J. Robust deadbeat predictive direct speed control for PMSM with dual second-order sliding-mode disturbance observers and sensitivity analysis. *IEEE Trans. Power Electron.* **2023**, *38*, 8310–8326. [CrossRef]
16. Kawai, H.; Zhang, Z.; Kennel, R.; Doki, S. Direct speed control based on finite control set model predictive control with voltage smoother. *IEEE Trans. Ind. Electron.* **2022**, *70*, 2363–2372. [CrossRef]
17. Zhang, X.; He, Y. Direct voltage-selection based model predictive direct speed control for PMSM drives without weighting factor. *IEEE Trans. Power Electron.* **2018**, *34*, 7838–7851. [CrossRef]
18. Wang, Z.; Chai, J.; Xiang, X.; Sun, X.; Lu, H. A novel online parameter identification algorithm designed for deadbeat current control of the permanent-magnet synchronous motor. *IEEE Trans. Ind. Appl.* **2021**, *58*, 2029–2041. [CrossRef]
19. Feng, G.; Lai, C.; Tan, X.; Wang, B.; Kar, N.C. Optimal current modeling and identification for fast and efficient torque ripple minimization of PMSM using theoretical and experimental models. *IEEE Trans. Ind. Electron.* **2020**, *68*, 11806–11816. [CrossRef]
20. Liu, H.; Lin, W.; Liu, Z.; Buccella, C.; Cecati, C. Model predictive current control with model-aid extended state observer compensation for PMSM drive. *IEEE Trans. Power Electron.* **2022**, *38*, 3152–3162. [CrossRef]
21. Wang, F.; He, L. FPGA-based predictive speed control for PMSM system using integral sliding-mode disturbance observer. *IEEE Trans. Ind. Electron.* **2020**, *68*, 972–981. [CrossRef]
22. Gao, F.; Yin, Z.; Li, L.; Li, T.; Liu, J. Gaussian noise suppression in deadbeat predictive current control of permanent magnet synchronous motors based on augmented fading Kalman filter. *IEEE Trans. Energy Convers.* **2022**, *38*, 1410–1420. [CrossRef]
23. Alma, Y.A.; Gustavo, M.-G.; Jorge, R. Nested High Order Sliding Mode Controller with Back-EMF Sliding Mode Observer for a Brushless Direct Current Motor. *Electronics* **2020**, *9*, 1041. [CrossRef]
24. Du, S.; Liu, Y.; Wang, Y.; Li, Y.; Yan, Z. Research on a Permanent Magnet Synchronous Motor Sensorless Anti-Disturbance Control Strategy Based on an Improved Sliding Mode Observer. *Electronics* **2023**, *12*, 4188. [CrossRef]
25. Yao, G.; Gao, J.; Lei, J.; Han, S.; Xiao, Y. Design of Fractional-Order Non-Singular Terminal Sliding Mode Observer Sensorless System for Surface-Mounted Permanent Magnet Synchronous Motor. *Electronics* **2024**, *13*, 1601. [CrossRef]
26. Tang, P.; Dai, Y.; Li, Z. Unified Predictive Current Control of PMSMs with Parameter Uncertainty. *Electronics* **2019**, *8*, 1534. [CrossRef]
27. Zhu, Y.; Tao, B.; Xiao, M.; Yang, G.; Zhang, X.; Lu, K. Luenberger Position Observer Based on Deadbeat-Current Predictive Control for Sensorless PMSM. *Electronics* **2020**, *9*, 1325. [CrossRef]
28. Mohamed, A.; Christoph, H.; Ralph, K. Robust Predictive Control Scheme for Permanent-Magnet Synchronous Generators Based Modern Wind Turbines. *Electronics* **2021**, *10*, 1596. [CrossRef]
29. Zhang, X.; Cheng, Y.; Zhao, Z.; He, Y. Robust Model Predictive Direct Speed Control for SPMSM Drives Based on Full Parameter Disturbances and Load Observer. *IEEE Trans. Power Electron.* **2020**, *35*, 8361–8373. [CrossRef]
30. Yang, L.; Li, H.; Huang, J.; Zhang, Z.; Zhao, H. Model Predictive Direct Speed Control with Novel Cost Function for SMPMSM Drives. *IEEE Trans. Power Electron.* **2022**, *37*, 9586–9596. [CrossRef]
31. Yim, J.; You, S.; Lee, Y.; Kim, W. Chattering attenuation disturbance observer for sliding mode control: Application to permanent magnet synchronous motors. *IEEE Trans. Ind. Electron.* **2022**, *70*, 5161–5170. [CrossRef]

32. Kashif, M.; Singh, B. Modified active-power MRAS based adaptive control with reduced sensors for PMSM operated solar water pump. *IEEE Trans. Energy Convers.* **2022**, *38*, 38–52. [CrossRef]
33. Lu, W.; Tang, B.; Ji, K.; Lu, K.; Wang, D.; Yu, Z. A new load adaptive identification method based on an improved sliding mode observer for PMSM position servo system. *IEEE Trans. Power Electron.* **2020**, *36*, 3211–3223. [CrossRef]

Disclaimer/Publisher's Note: The statements, opinions and data contained in all publications are solely those of the individual author(s) and contributor(s) and not of MDPI and/or the editor(s). MDPI and/or the editor(s) disclaim responsibility for any injury to people or property resulting from any ideas, methods, instructions or products referred to in the content.